Tracking isotopically labeled oxidants using boronate-based redox probes

Received for publication, March 10, 2020, and in revised form, March 26, 2020 Published, Papers in Press, March 26, 2020, DOI 10.1074/jbc.RA120.013402

Natalia Rios[‡§], Rafael Radi[‡§], Balaraman Kalyanaraman[¶], and Jacek Zielonka[¶1]

From the [‡]Departamento de Bioquímica, [§]Centro de Investigaciones Biomédicas (CEINBIO), Facultad de Medicina, Universidad de la República, 11800 Montevideo, Uruguay and [¶]Department of Biophysics, Medical College of Wisconsin, Milwaukee, Wisconsin 53226

Edited by F. Peter Guengerich

Reactive oxygen and nitrogen species have been implicated in many biological processes and diseases, including immune responses, cardiovascular dysfunction, neurodegeneration, and cancer. These chemical species are short-lived in biological settings, and detecting them in these conditions and diseases requires the use of molecular probes that form stable, easily detectable, products. The chemical mechanisms and limitations of many of the currently used probes are not well-understood, hampering their effective applications. Boronates have emerged as a class of probes for the detection of nucleophilic two-electron oxidants. Here, we report the results of an oxygen-18–labeling MS study to identify the origin of oxygen atoms in the oxidation products of phenylboronate targeted to mitochondria. We demonstrate that boronate oxidation by hydrogen peroxide, peroxymonocarbonate, hypochlorite, or peroxynitrite involves the incorporation of oxygen atoms from these oxidants. We therefore conclude that boronates can be used as probes to track isotopically labeled oxidants. This suggests that the detection of specific products formed from these redox probes could enable precise identification of oxidants formed in biological systems. We discuss the implications of these results for understanding the mechanism of conversion of the boronate-based redox probes to oxidant-specific products.

Reactive oxygen species (ROS),[2] including superoxide ($O_2^{\bullet-}/HO_2^{\bullet}$), hydrogen peroxide ($H_2O_2$), and peroxynitrite ($ONOO^-/ONOOH$), have been implicated in (patho)physiological mechanisms in redox biology and medicine (1–4). Both superoxide and H_2O_2 are relatively slow reacting and/or weak oxidants (4–6) but in biological systems can be converted to more reactive species (see Fig. 1), including peroxynitrite (7, 8), peroxymonocarbonate (HCO_4^-) (9, 10), or hypochlorous acid (HOCl) (11), resulting in enhanced redox signaling and/or damage to cell components (5, 12, 13). Because of the short lifetime of most ROS in biological settings, detection and quantitative analyses of those species have remained a challenge, and development of new probes for redox biology is an active area of research. Most chemical probes used for the detection of cellular oxidants lack selectivity toward a single species. For example, dichlorodihydrofluorescein (DCFH), dihydrorhodamine-123 (DHR123), and Amplex Red undergo two-electron oxidation to fluorescent dichlorofluorescein, rhodamine, and resorufin, respectively, and nitro blue tetrazolium undergoes four-electron reduction to diformazan, without incorporation of the reactive species detected into the product formed (Fig. 1). This often leads to ambiguity regarding the identity of the species detected and prevents tracking of the oxidants using isotope-labeling approach. ROS detection and their unambiguous identification in biological systems requires the use of chemical probes, which upon reaction form species-specific product(s) (14–19). As an example, spin traps react with most radicals by the formation of a covalent bond between the probe and the radical trapped, and the product formed is typically highly specific for the trapped species. Also, the conversion of hydroethidine (HE) into 2-hydroxyethidium (2-OH-E^+) has been used to detect $O_2^{\bullet-}$ in cultured cells *in vitro* and in animal models *in vivo* (20–27). Other products formed from the HE probe, including diethidium and 2-chloroethidium (2-Cl-E^+), have been proposed as specific marker products of one-electron oxidants and hypochlorous acid, respectively (28, 29).

Oxidation of boronate-based probes into phenolic products has been utilized for the detection of H_2O_2 (30–32). An array of boronate probes, with similar chemical reactivities and a similar mechanism of response to H_2O_2 but with different modes of detection, has been reported (33–37). Also, fluorogenic boronate probes targeted to various subcellular compartments have been described (31, 38–40). Triphenylphosphonium (TPP^+)-conjugated phenylboronic acid (called MitoB) was designed for MS-based detection of mitochondrial H_2O_2 (41–43). Resistance of boronates to heme-catalyzed oxidation makes them

This work was supported by NCI, National Institutes of Health Grants U01CA178960 and R01CA208648 (to B. K.) and by Espacio Interdisciplinario 2015 and CSIC Grupos 2018, Universidad de la República, Uruguay (to R. R.). This work was also supported by American Cancer Society Institutional Research Grant IRG 16-183-31 and the MCW Cancer Center (to J. Z.); by Agencia Nacional de Investigación e Innovación (ANII) and Universidad de la República fellowships (to N. R.); and by Programa de Desarrollo de Ciencias Básicas (PEDECIBA, Uruguay) (to R. R. and N. R.). The authors declare that they have no conflicts of interest with the contents of this article. The content is solely the responsibility of the authors and does not necessarily represent the official views of the National Institutes of Health.
This article contains Fig. S1.

[1] To whom correspondence should be addressed: 8701 Watertown Plank Road, Milwaukee, WI 53226. Tel.: 414-955-4789; E-mail: jzielonk@mcw.edu.

[2] The abbreviations used are: ROS, reactive oxygen species; 2-Cl-E^+, 2-chloroethidium; DCFH, dichlorodihydrofluorescein; DHR123, dihydrorhodamine-123; dtpa, diethylenetriamine pentaacetic acid; HE, hydroethidine; HPLC, high-performance LC; HX, hypoxanthine; MeCN, acetonitrile; MPO, myeloperoxidase; MRM, multiple reaction monitoring; 2-OH-E^+, 2-hydroxyethidium; *o*MitoPhB$(OH)_2$, mitochondria-targeted phenyl boronate probe; SOD, superoxide dismutase; TPP^+, triphenylphosphonium cationic moiety; XO, xanthine oxidase

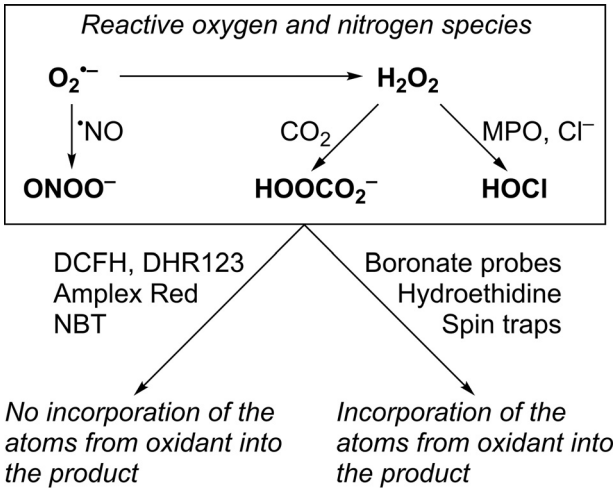

Figure 1. In contrast to commonly used redox probes DCFH, DHR123, Amplex Red, and NBT, spin traps, boronate-based probes, and HE incorporate atoms from the oxidants into the products formed.

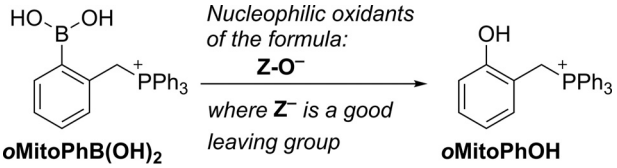

Figure 2. Conversion of *o*MitoPhB(OH)$_2$ boronate probe in the phenolic product, *o*MitoPhOH, in the presence of nucleophilic two-electron oxidants.

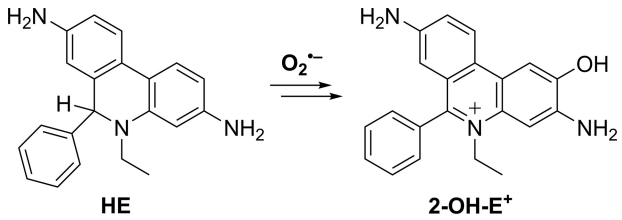

Figure 3. Conversion of HE into 2-OH-E$^+$ by $O_2^{\bullet-}$.

good candidates for the detection of oxidants in the *in vivo* settings. Boronate-based probes are oxidized more than a thousand times faster by HOCl and nearly a million times faster by $ONOO^-$ than by H_2O_2 ($k_{H2O2} \sim 1\ M^{-1}s^{-1}$; $k_{HOCl} \sim 10^4\ M^{-1}s^{-1}$; $k_{ONOO-} \sim 10^6\ M^{-1}s^{-1}$), and the reaction typically involves a minor pathway, with the formation of $ONOO^-$-specific product(s) (7, 44–48). Recently, it has been reported that peroxymonocarbonate, the product of the reaction of H_2O_2 with CO_2, reacts with coumarin boronic acid nearly 50 times faster than H_2O_2 ($k_{HCO4-} \sim 10^2\ M^{-1}s^{-1}$) (10).

Although the identities of the oxidation, chlorination, and nitration products of boronate probes have been established in many cases, and the reaction mechanisms have been proposed, the origin of oxygen atoms in the oxidation and nitration products of boronate probes has not been experimentally determined. Understanding the mechanisms of formation of the oxidation products is required for their rigorous use as specific ROS markers in the *in vitro* and *in vivo* settings. Also, the potential for selective monitoring of the specific oxidizing species, through use of isotopically labeled oxidant and monitoring isotopic labeling of the specific products, remains to be explored.

Here, we report on the incorporation of an oxygen atom from the biologically relevant two-electron oxidants, including H_2O_2, HCO_4^-, HOCl, and $ONOO^-$ in the oxidation and nitration products of the mitochondria-targeted phenyl boronate probe (*o*MitoPhB(OH)$_2$) (Fig. 2). In addition, we demonstrate the involvement of oxygen atoms from superoxide in the formation of the hydroxylated product, 2-OH-E$^+$, during oxidation of hydroethidine by $O_2^{\bullet-}$ (Fig. 3), corroborating the proposed mechanism of the conversion of HE into 2-OH-E$^+$.

Results

We have investigated the incorporation of oxygen atoms from different biologically relevant nucleophilic oxidants (Fig. 1) capable of oxidizing boronate probes into the products formed. We chose *o*MitoPhB(OH)$_2$ as a model boronate probe (Fig. 2) because its reactivity toward H_2O_2, HOCl, and $ONOO^-$ has been studied previously in detail and the products characterized (49–51). To demonstrate the formation of ^{18}O-labeled superoxide, we have also tracked the incorporation of the ^{18}O atom into the hydroxylation product of hydroethidine.

Hydrogen peroxide

Upon oxidation by H_2O_2, a conversion of *o*MitoPhB(OH)$_2$ into the phenolic product (*o*MitoPhOH) occurs (Fig. 4). H_2O_2 oxidizes the phenylboronate substrate into a phenoxyboronate intermediate that, upon hydrolysis, yields the phenolic product and boric acid. To determine whether the phenolic oxygen atom derives from H_2O_2 or water, we performed the oxidation of *o*MitoPhB(OH)$_2$ by $H_2{}^{16}O_2$ in $H_2{}^{18}O$ and by $H_2{}^{18}O_2$ in $H_2{}^{16}O$ (Fig. 5). The product detected in the presence of $H_2{}^{16}O_2$ showed the molecular mass of *o*MitoPh^{16}OH (m/z = 369); in the presence of $H_2{}^{18}O_2$, the product had a molecular mass of 371 (Fig. 5, *a* and *b*), attributed to *o*MitoPh^{18}OH. Liquid chromatography with tandem MS (LC-MS/MS) analyses indicated no formation of *o*MitoPh^{18}OH during the oxidation of the probe by $H_2{}^{16}O_2$ in $H_2{}^{18}O$, whereas it was the predominant product in the presence of $H_2{}^{18}O_2$ (Fig. 5*c*). We conclude that during oxidation of boronates by H_2O_2, the oxygen atom in the phenolic product derives exclusively from H_2O_2 and not from water.

Peroxymonocarbonate

In the presence of CO_2, H_2O_2 is in equilibrium with a more potent oxidant, peroxymonocarbonate ($HOOCO_2^-$) (Fig. 6*a*) (9, 52, 53). Formation of this species has been implicated, for example, in the enhanced hyperoxidation of cellular peroxiredoxins and protein tyrosine phosphatase 1B–mediated signaling cascade observed in the presence of bicarbonate (12, 54–56). Recently, it was shown that the rate of oxidation of the coumarin boronate probe in the presence of H_2O_2 is increased after the addition of bicarbonate (10). Therefore, we tested if the H_2O_2-derived HCO_4^- incorporates the oxygen atom into *o*MitoPhB(OH)$_2$ probe.

First, we confirmed that the experimental conditions we used would allow us to detect increased formation of the phenolic product during the reaction of the probe with H_2O_2 upon addition of $NaHCO_3$. In fact, with increased concentration of $NaHCO_3$, the rate of product formation increased, as determined by LC-MS–based monitoring of the accumulation of

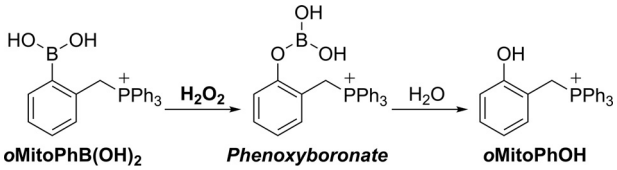

Figure 4. Oxidation of the *o*MitoPhB(OH)$_2$ probe by H_2O_2.

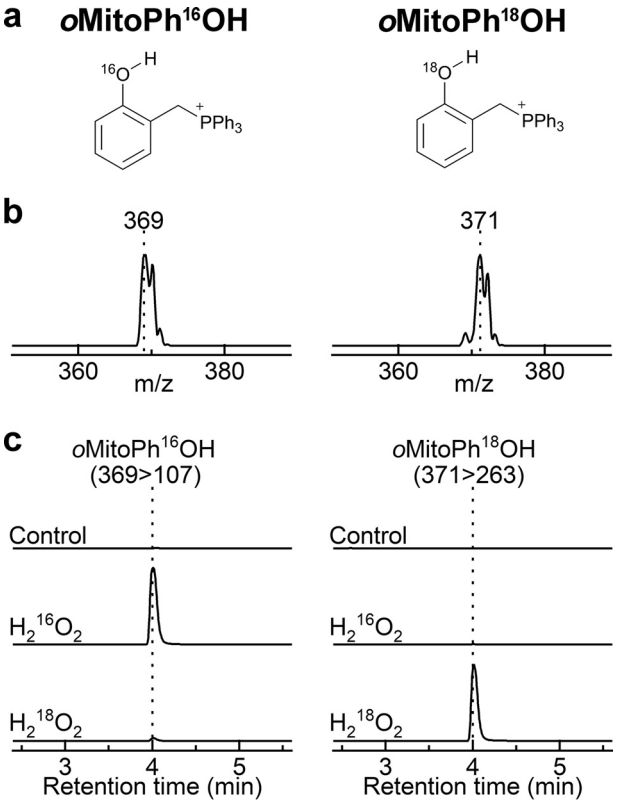

Figure 5. Incorporation of an oxygen atom into the phenolic product during the oxidation of *o*MitoPhB(OH)$_2$ by H_2O_2. *a*, chemical structures of the products. *b*, online mass spectra of the products. *c*, LC-MS/MS traces of the phenolic products containing ^{16}O (*left panel*) or ^{18}O (*right panel*). LC-MS/MS analyses were performed after incubation (20 min) of *o*MitoPhB(OH)$_2$ (20 μM) alone (control), with $H_2{}^{16}O_2$ (10 mM) in $H_2{}^{18}O$ (90%), or with $H_2{}^{18}O_2$ (10 mM) in $H_2{}^{16}O$.

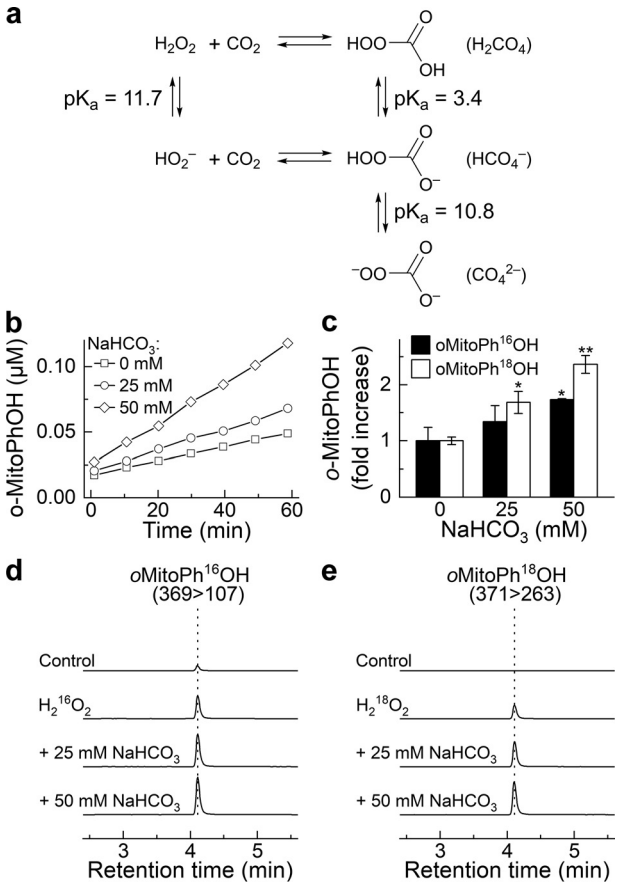

Figure 6. NaHCO$_3$-enhanced oxidation of *o*MitoPhB(OH)$_2$ by H_2O_2 and incorporation of an oxygen atom from HCO_4^- into the phenolic product. *a*, chemical scheme of the formation of HCO_4^- and acid-base equilibria involved. *b*, dynamics of the formation of *o*MitoPhOH in the absence and presence of NaHCO$_3$. *c*, relative increase in the yield of *o*MitoPhOH after 1-h incubation of the probe with $H_2{}^{16}O_2$ or $H_2{}^{18}O_2$ in the absence and presence of NaHCO$_3$. *d* and *e*, LC-MS/MS traces of the phenolic products containing ^{16}O (*d*) or ^{18}O (*e*) atoms. LC-MS/MS analyses were performed after incubation (1 h) of *o*MitoPhB(OH)$_2$ (1 μM) alone (control), with $H_2{}^{16}O_2$ (50 μM, *d*), or with $H_2{}^{18}O_2$ (50 μM, *e*). All solutions contained 0.1 M phosphate buffer and 0.1 mM dtpa, and the pH of the solutions was adjusted to 7.0.

*o*MitoPhOH over the incubation time (Fig. 6, *b* and *c*). This effect was observed for both $H_2{}^{16}O_2$ and $H_2{}^{18}O_2$, when monitoring the ^{16}O- or ^{18}O-phenolic products, respectively (Fig. 6*c*). The relative increase in the yield of the phenolic product in the case of *o*MitoPh^{18}OH was higher than in case of *o*MitoPh^{16}OH, which we attribute to the presence of small amounts of *o*MitoPh^{16}OH but not *o*MitoPh^{18}OH in the probe stock solution. The representative LC-MS chromatograms for both $H_2{}^{16}O_2$ and $H_2{}^{18}O_2$, with increased concentrations of NaHCO$_3$ are shown in Fig. 6, *d* and *e*. Under those conditions, $HC^{16}O_4^-$ and $HC^{18}O_2{}^{16}O_2^-$ were formed, respectively. Incorporation of an ^{18}O atom into the phenolic product indicates the involvement of the peroxyl moiety of HCO_4^- in the oxidation reaction. Obtained data are consistent with the addition of the deprotonated form of peroxymonocarbonate (CO_4^{2-}) to the boronate moiety, with elimination of the carbonate anion and incorporation of an oxygen atom from the peroxyl part of the oxidant.

Hypochlorite

Boronates are oxidized more than a thousand times faster by HOCl than by H_2O_2 at neutral pH (44). The product of the reaction is a phenol (or alcohol), which may undergo chlorination in the presence of excess HOCl (47, 51, 57). To determine the source of the oxygen atom during the conversion of *o*MitoPhB(OH)$_2$ into *o*MitoPhOH, we generated H^{16}OCl and H^{18}OCl *in situ* from myeloperoxidase (MPO)-catalyzed oxidation of chloride anions by $H_2{}^{16}O_2$ and $H_2{}^{18}O_2$, respectively (Fig. 7*a*). To confirm the formation of HOCl in the investigated system, we also performed similar incubations using $H_2{}^{18}O_2$ in the presence of the HE probe, and monitored the chlorination product, 2-Cl-E$^+$ (29).

Incubation of *o*MitoPhB(OH)$_2$ with H_2O_2, MPO, and potassium chloride (KCl) led to a significant increase in the production of the phenolic product, confirming that HOCl was the major species responsible for oxidation under the conditions used (Fig. 7*b*). The omission of KCl or MPO resulted in a significantly lower yield of the product. Also, addition of small amounts of dimethyl sulfoxide (DMSO), known to rapidly scav-

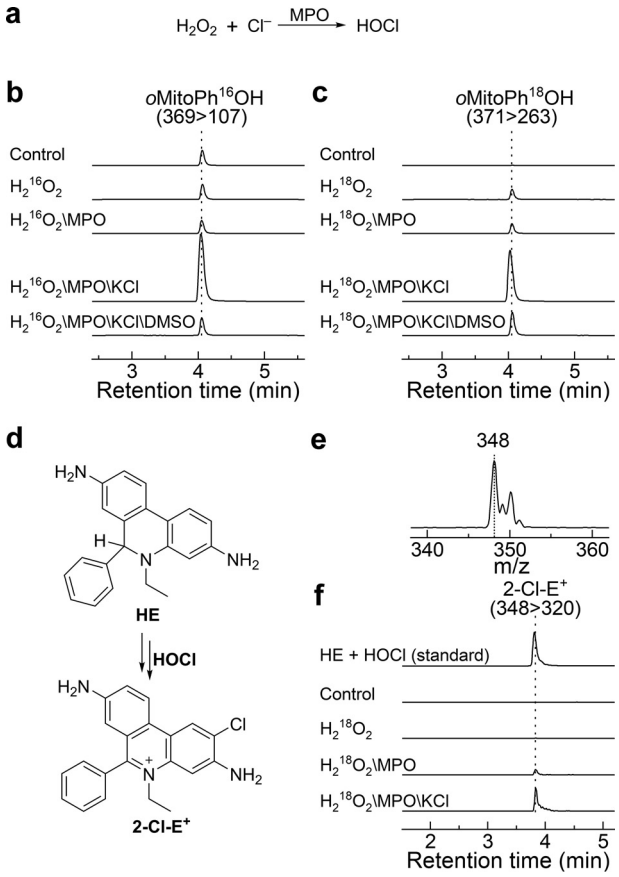

Figure 7. Incorporation of an oxygen atom into the phenolic product during oxidation of *o*MitoPhB(OH)$_2$ by HOCl. *a*, method generating HOCl. *b* and *c*, LC-MS/MS traces of the phenolic products containing ^{16}O (*b*) or ^{18}O (*c*). LC-MS/MS analyses were performed after incubation (15 min) of *o*MitoPhB(OH)$_2$ (50 μM) alone (control), with $H_2{}^{16}O_2$ (0.1 mM, *b*), or with $H_2{}^{18}O_2$ (0.1 mM, *c*) in the presence or absence of MPO (20 nM) and KCl (0.1 M). All solutions contained 0.1 M phosphate buffer, pH 7.4. *d*, scheme of the conversion of HE into 2-Cl-E$^+$. *e*, online mass spectrum of 2-Cl-E$^+$ detected from reaction of HE with bolus HOCl. *f*, confirmation of HOCl generation using 2-Cl-E$^+$ marker product. All experimental conditions were the same as described above, but the *o*MitoPhB(OH)$_2$ probe was replaced by HE (50 μM).

enge HOCl (47, 58), led to a significant attenuation of the formation of the phenolic product. Formation of HOCl was further confirmed by the detection of 2-Cl-E$^+$ in analogous systems, using the HE probe instead of the boronate (Fig. 7, *d–f*). It previously was shown that HOCl and taurine chloramine are able convert HE into 2-Cl-E$^+$ (29).

Replacement of $H_2{}^{16}O_2$ with $H_2{}^{18}O_2$ in the incubation mixture containing *o*MitoPhB(OH)$_2$, MPO, and KCl resulted in a switch from *o*MitoPh^{16}OH to *o*MitoPh^{18}OH (Fig. 7*c*). In the case of both isotopologs, the signal was maximal in a mixture containing H_2O_2, MPO, and KCl and decreased upon the addition of DMSO. We conclude that the oxygen atom in the product of *o*MitoPhB(OH)$_2$ oxidation by HOCl derives from the oxidant.

Peroxynitrite

Similar to H_2O_2, $ONOO^-$ reacts with boronates to form a corresponding phenol as the major product. The rate constant of the reaction, however, is significantly higher ($\sim 10^6$ $M^{-1}s^{-1}$ for $ONOO^-$ and ~ 1 $M^{-1}s^{-1}$ for H_2O_2), and the reaction typically involves a minor pathway, leading to $ONOO^-$-specific

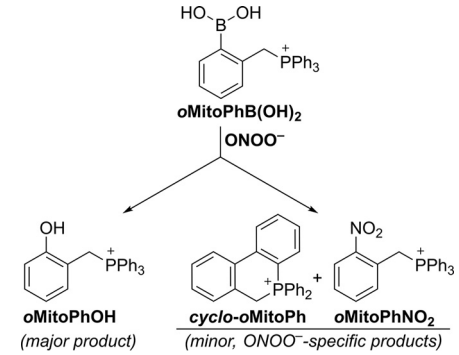

Figure 8. Oxidation of the *o*MitoPhB(OH)$_2$ probe by $ONOO^-$.

minor products (59). The high rate constant provides an opportunity to estimate the absolute flux of $ONOO^-$ in cultured cells (48, 60, 61). Formation of $ONOO^-$-specific products provides an opportunity to selectively monitor $ONOO^-$ formation in chemical and biological systems (14). We have previously applied this approach to demonstrate the formation of $ONOO^-$ during the reaction of nitroxyl with oxygen (62). In the case of oxidation of *o*MitoPhB(OH)$_2$ by $ONOO^-$, the minor products include *cyclo-o*MitoPh and *o*MitoPhNO$_2$ (Fig. 8), formed in 10 and 0.5% yields, respectively (51). Although the mechanism of the oxidation of boronates by $ONOO^-$ has been extensively studied, both experimentally and using theoretical calculations (44, 45, 47, 49), the isotope-labeling studies have not been performed. We decided to test the proposed reaction mechanism by reacting *o*MitoPhB(OH)$_2$ with ^{18}O-labeled $ONOO^-$, produced *in situ* from co-generated fluxes of nitric oxide ($^{\bullet}NO$) and $^{18}O_2^{\bullet-}$ (7, 8). $^{\bullet}NO$ flux was generated from the decomposition of spermine NONOate, whereas $^{18}O_2^{\bullet-}$ flux was produced during xanthine oxidase (XO)-catalyzed oxidation of hypoxanthine (HX) in the presence of $^{18}O_2$. The identity of $^{18}O_2^{\bullet-}$ has been confirmed by using the HE probe and monitoring the incorporation of ^{18}O atoms into the superoxide-specific product 2-OH-E$^+$ (see below). Co-generation of $^{\bullet}N^{16}O$ and $^{18}O_2^{\bullet-}$ leads to the formation of $^{16}ON^{18}O^{18}O^-$, providing an opportunity to track different oxygen atoms from $ONOO^-$ during the conversion of *o*MitoPhB(OH)$_2$ into *o*MitoPhOH and *o*MitoPhNO$_2$. Incubation of *o*MitoPhB(OH)$_2$ with ^{16}ON $^{18}O^{18}O^-$ led to the formation of the major phenolic product, which showed the mass (m/z = 371) to be two units higher than when using $^{16}ON^{16}O^{16}O^-$ (m/z = 369) (Fig. 9, *a* and *b*). LC-MS/MS traces of the phenolic products showed no formation of the *o*MitoPh^{18}OH in the presence of $^{16}ON^{16}O^{16}O^-$, although it was a predominant product when $^{16}ON^{18}O^{18}O^-$ was generated (Fig. 9*c*). In addition, changing the solvent to $H_2{}^{18}O$ failed to produce *o*MitoPh^{18}OH (Fig. S1). These data indicate that the formation of the phenolic product during the reaction of boronates with $ONOO^-$ is associated with the incorporation of the oxygen atom from the peroxyl part of the oxidant. Among the minor, $ONOO^-$-specific, products formed, *cyclo-o*MitoPh did not change its mass when switching from $^{16}ON^{16}O^{16}O^-$ to $^{16}ON^{18}O^{18}O^-$ (Fig. S1) as no oxygen atom is incorporated. *Cyclo-o*MitoPh was formed in maximal yields when $^{\bullet}NO$ and $O_2^{\bullet-}$ were co-generated, and its

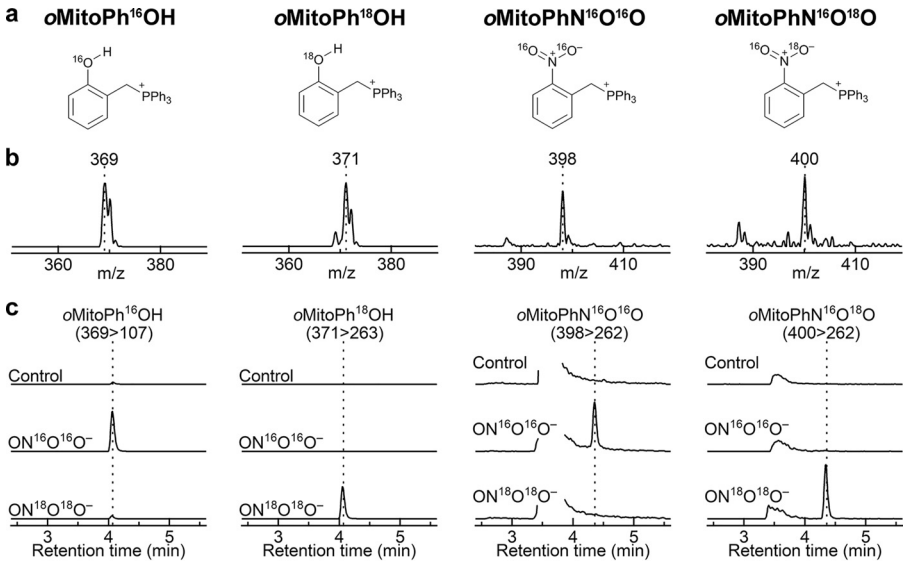

Figure 9. Incorporation of an oxygen atom into the phenolic and nitrated products during oxidation of *o*MitoPhB(OH)$_2$ by ONOO$^-$. *a*, chemical structures of the products. *b*, online mass spectra of the detected products. *c*, LC-MS/MS traces of the phenolic and nitrated products containing ^{16}O (*left panels*) or ^{18}O (*right panels*). LC-MS/MS analyses were performed after incubation (30 min) of *o*MitoPhB(OH)$_2$ (20 μM) alone (control) or with *in situ*–generated $ON^{16}O^{16}O^-$ or $ON^{18}O^{18}O^-$. $ON^{16}O^{16}O^-$ and $ON^{18}O^{18}O^-$ were produced by cogenerated fluxes of $^{\bullet}NO$ (0.2 μM/min) and $^{16}O_2^-$ or $^{18}O_2^-$ (0.2 μM/min), respectively.

peak intensity was similar for both $^{16}ON^{16}O^{16}O^-$ and $^{16}ON^{18}O^{18}O^-$ (Fig. S1).

Formation of the other minor product, *o*MitoPhNO$_2$, was associated with an increase in the mass of this product by two units (m/z = 400) in the presence of $^{16}ON^{18}O^{18}O^-$ as compared with the product formed by $^{16}ON^{16}O^{16}O^-$ (m/z = 398) (Fig. 9, *a* and *b*). This indicates that only one oxygen atom originated from the peroxyl (^{18}O-labeled) part of ONOO$^-$. Analyses of the LC-MS/MS traces indicate that *o*MitoPhN^{16}O^{18}O was formed only when $^{16}ON^{18}O^{18}O^-$ was produced (Fig. 9*c*), and *o*MitoPhN^{16}O$_2$ was the product of the reaction with $^{16}ON^{16}O^{16}O^-$, even when the reaction was carried out in $H_2{}^{18}O$ (Fig. S1). The data on the oxidation of *o*MitoPhB(OH)$_2$ by ONOO$^-$ indicate that the oxygen atoms introduced into the products originate from the oxidant and not from the solvent. These data are consistent with the occurrence of two reaction pathways, including heterolytic and homolytic cleavage of the peroxyl bond in the adduct of ONOO$^-$ to the boronate probe (Fig. 10). The major pathway, involving a heterolytic cleavage, leads to the formation of the phenolic product, with the oxygen atom incorporated from the peroxyl moiety of the oxidant, similar to the reaction with other tested oxidants, H_2O_2, $HCO_4{}^-$, and HOCl. The minor pathway, involving the homolytic cleavage of the peroxyl bond, leads to the formation of $^{\bullet}NO_2$ and a phenyl-type radical, which recombine within the solvent cage to form a nitrobenzene-type product (*o*MitoPhNO$_2$) (Fig. 10). The intramolecular addition of the phenyl radical to the phenyl ring of the TPP$^+$ moiety yields the cyclic product (*cyclo-o*MitoPh) without incorporating any atom from the oxidant.

Superoxide

The production of $^{16}ON^{18}O^{18}O^-$ for the study of the oxidation of boronates by ONOO$^-$ involved co-generation of $^{\bullet}NO$ and $^{18}O_2^-$. To confirm the formation of $^{18}O_2^-$ in the incubation mixture containing HX, XO, and $^{18}O_2$, we performed the incubation in the presence of the HE probe and monitored the incorporation of ^{18}O atoms into the 2-OH-E$^+$ product. HE is the most widely used probe for the detection of O_2^- in biological systems ranging from cultured cells to animals (21, 63). In the presence of O_2^-, HE is oxidized to 2-OH-E$^+$, a specific marker product for O_2^- (Fig. 3) (20–24). Derivatives of HE for site-specific detection of O_2^- have been reported (64–66). Those probes share the same oxidative chemistry with HE (65). A multistep mechanism of the conversion of HE to 2-OH-E$^+$ has been proposed that involves the oxidation of HE to the HE radical cation (HE$^{\bullet+}$), followed by the reaction of HE$^{\bullet+}$ with O_2^- to form 2-OH-E$^+$ (21, 67). This has been supported by pulse radiolysis data, showing the formation and rapid decay of HE$^{\bullet+}$ in the presence of pulse-generated O_2^- (68) and an increase in the yield of 2-OH-E$^+$ by the addition of peroxidase in the presence of a steady flux of O_2^- (67). Here, we provide direct proof of the production of $^{18}O_2^-$ in the HX/XO/$^{18}O_2$ system and the incorporation of the oxygen atom from O_2^- into the product during oxidation of HE to 2-OH-E$^+$.

To follow the oxygen atoms, we incubated HE with $^{16}O_2^-$ or $^{18}O_2^-$, produced during enzymatic oxidation of HX by XO in the presence of $^{16}O_2$ or $^{18}O_2$, and monitored the formation of 2-^{16}OH-E$^+$ and 2-^{18}OH-E$^+$ (Fig. 11*a*). The mass spectra of the products showed m/z values of 330 and 332 when the probe was incubated with $^{16}O_2^-$ or $^{18}O_2^-$, respectively (Fig. 11*b*). The increase in the mass of the product from $^{18}O_2^-$ is consistent with incorporation of ^{18}O into the molecule. The LC-MS/MS traces (Fig. 11*c*) indicate significant formation of 2-^{16}OH-E$^+$ and negligible formation of 2-^{18}OH-E$^+$ in the presence of $^{16}O_2^-$ (HX/XO/$^{16}O_2$). In the presence of $^{18}O_2^-$ (HX/XO/$^{18}O_2$), only a small peak of 2-^{16}OH-E$^+$ and an intense peak because of 2-^{18}OH-E$^+$ were observed. Furthermore, incubation of HE with $^{16}O_2^-$ in a solvent containing 90% of $H_2{}^{18}O$ led to the formation of 2-^{16}OH-E$^+$ but not 2-^{18}OH-E$^+$ (not shown). These data confirm the formation of $^{18}O_2^-$ in the HX/XO/$^{18}O_2$ system and indicate that during the oxidation and hydroxylation of HE, the

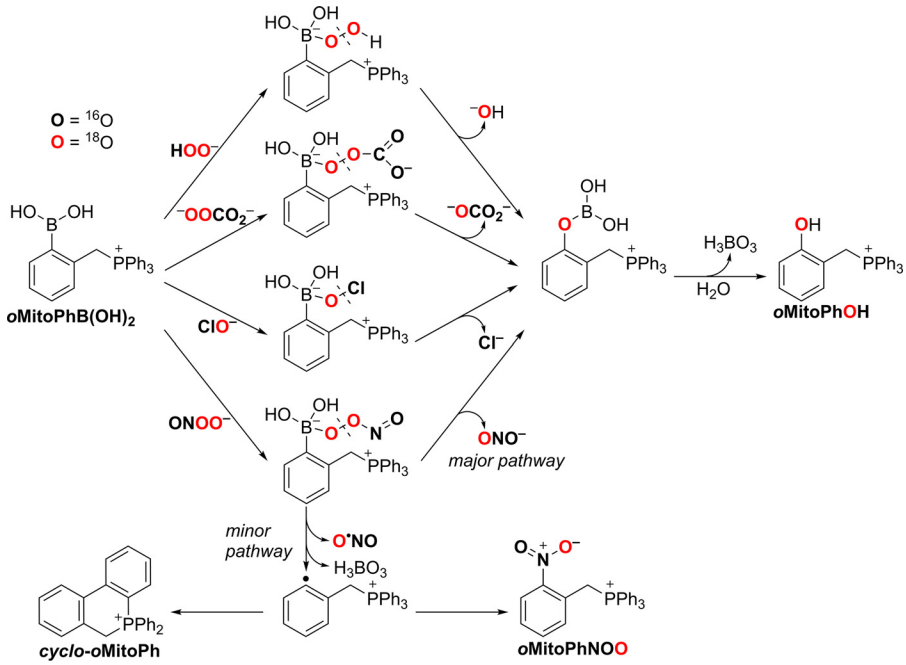

Figure 10. Proposed mechanism of incorporation of oxygen atoms into the oxidation and nitration products of *o*MitoPhB(OH)$_2$ from H_2O_2, HCO_4^-, HOCl, and $ONOO^-$.

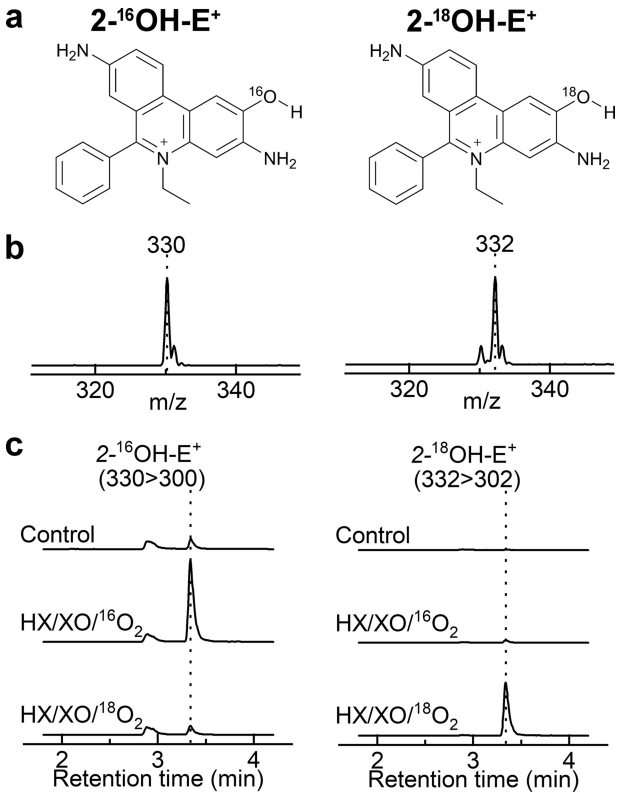

Figure 11. Incorporation of an oxygen atom into the hydroxylated product during oxidation of HE in the presence of $O_2^{\bullet-}$. *a*, chemical structures of the products. *b*, online mass spectra of the products. *c*, LC-MS/MS traces of 2-OH-E$^+$ containing ^{16}O (*left panel*) or ^{18}O (*right panel*). LC-MS/MS analyses were performed after incubation (30 min) of HE (20 μM) alone (control) or with $^{16}O_2^{\bullet-}$ or $^{18}O_2^{\bullet-}$ (0.2 μM $O_2^{\bullet-}$/min, generated from HX/XO and $^{16}O_2$ or $^{18}O_2$, respectively).

oxygen atom in the product originates from $O_2^{\bullet-}$, consistent with a mechanism involving the reaction of $HE^{\bullet+}$ with $O_2^{\bullet-}$ and forming the hydroperoxyl intermediate (Fig. 12).

Discussion

Isotope tracing is a powerful technique in the study of the mechanism of chemical and enzymatic reactions as well as cellular metabolism (69–71). Isotopically labeled oxidants have been used to identify the spin adducts of $O_2^{\bullet-}$ and other oxygen-centered radicals using an EPR spin trapping technique (72). EPR spin trapping, however, is only useful for the detection of radical species and has only limited applicability to detect intracellular ROS. Oxygen tracing in other probes used for cellular oxidants has not been reported.

In this study, we have investigated the origin of the oxygen atom in the products of the reaction of mitochondria-targeted boronate probe with four biologically relevant, two-electron oxidants: hydrogen peroxide, peroxymonocarbonate, hypochlorite, and peroxynitrite. The results support the previously proposed mechanisms of the probes' oxidation and formation of the specific products and provide a solid foundation for the use of those products for identification and tracking isotopically labeled oxidants.

New insights into the selective detection of peroxynitrite

Although initially assumed to be completely selective (specific) for H_2O_2, boronate-based probes also respond to other biologically relevant nucleophilic oxidants, including HCO_4^-, HOCl, $ONOO^-$, and amino acid hydroperoxides (44, 57, 73). The main oxidation product in case of all the listed oxidants is the corresponding phenol. In the presence of excess HOCl or $ONOO^-$, the phenolic product may undergo chlorination or nitration, respectively, providing an opportunity to identify the oxidant by profiling the products formed (14, 44). As an example, in the presence of HOCl, the peroxy-caged luciferin probe is converted not only to luciferin but also to chloroluciferin (47). The reaction of boronate probes with $ONOO^-$ is of special interest, as this reaction typically proceeds via two pathways of

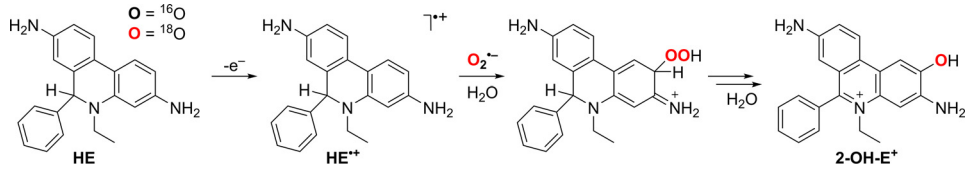

Figure 12. Proposed mechanism of incorporation of oxygen atom from $O_2^{\bullet-}$ into 2-OH-E^+ during oxidation of the HE probe.

the decomposition of peroxynitrite adduct to the boronate: (i) major pathway (~85–90%) involving heterolytic cleavage of the peroxyl bond, leading to the formation the phenolic product and (ii) minor pathway (10–15%), involving a homolytic cleavage of the peroxyl bond, with the formation of phenyl-type radical and $^{\bullet}NO_2$, which upon recombination form nitrobenzene-type product (Fig. 10) (45). We have proposed using that product as a specific marker for $ONOO^-$ (50), and with such an approach, we demonstrated the formation of $ONOO^-$ during the reaction of nitroxyl with oxygen (O_2) (62). In the case of the *o*MitoPhB$(OH)_2$ probe, the nitrated product, *o*MitoPhNO_2, accounts for only 0.5% of $ONOO^-$ consumed. The other minor product, *cyclo-o*MitoPh, is formed at 10% yield, via a rapid intramolecular addition of the phenyl-type radical to one of the phenyl rings of the TPP^+ moiety (Fig. 10) (51). Both minor products have been detected in macrophages stimulated to produce $ONOO^-$ (51) and can be used as specific marker products for intracellular $ONOO^-$.

Detection of $ONOO^-$ in cells has remained a challenge, as most methods were based on the nitrative and/or oxidative properties of $ONOO^-$-derived radicals (*e.g.* $^{\bullet}OH$, $^{\bullet}NO_2$, $CO_3^{\bullet-}$) (74). However, the same radical species can be formed in biological systems in $ONOO^-$-independent reactions. For example, although nitrated tyrosine residues are commonly used as an endogenous marker of $ONOO^-$, the same product is formed by $^{\bullet}NO_2$ from the MPO-catalyzed oxidation of nitrite by H_2O_2. Dihydrorhodamine, a fluorogenic probe used for $ONOO^-$ detection, cannot distinguish the two pathways of $^{\bullet}NO_2$ formation either. Boronate probes, including *o*MitoPhB$(OH)_2$ provide the first chemical tool to distinguish these two nitration pathways (51). Formation of the cyclic and nitrobenzene-type products from *o*MitoPhB$(OH)_2$ occurs in the presence of $ONOO^-$ but not in the presence of MPO/H_2O_2/NO_2^- (51). This shows that monitoring the conversion of *o*MitoPhB$(OH)_2$ into *cyclo-o*MitoPh and *o*MitoPhNO_2 products can be used to selectively detect $ONOO^-$ formed in cell-free and cellular systems. Although other boronate probes may not form the cyclic product during the reaction with $ONOO^-$, in most cases they produce nitrobenzene-type minor products. These products may be used to confirm the identity of the oxidant detected. For example, a new boronate probe recently was developed to detect $ONOO^-$ in β-amyloid aggregates (76). The minor product(s) formed during the reaction of the probe with $ONOO^-$ should be characterized and high-performance LC (HPLC)– or LC-MS–based profiling should accompany fluorescence measurements, which report the yield of the phenolic product. This product is common for various nucleophilic oxidants, as exemplified here by H_2O_2, HCO_4^-, HOCl, and $ONOO^-$. Amino acid– and protein-based hydroperoxides also oxidize boronate probes to the phenolic products (73).

Oxidation of aromatic boronates involves initial formation of phenoxyboronic acid, followed by its hydrolysis into phenolic product (Fig. 4). The results obtained in this study demonstrate that during the oxidation of boronates by H_2O_2, HCO_4^-, HOCl, or $ONOO^-$, the oxygen atom in the phenolic product derives from those oxidants, not from water. In the case of HCO_4^- and $ONOO^-$, the oxygen atoms in these oxidants are not equivalent, and the data obtained support the mechanism involving the nucleophilic addition of CO_4^{2-} or $ONOO^-$ to the boron atom, via their peroxyl moieties, followed by elimination of a carbonate or nitrite anion, respectively (Fig. 10). Also, in the case of the formation of nitrobenzene-type product, the pattern of labeling of *o*MitoPhNO_2 during the reaction of *o*MitoPhB$(OH)_2$ with $ONOO^-$ provides insight into the mechanism of the minor pathway of the reaction. Incorporation of only one oxygen-18 atom into the nitrated product from $^{16}ON^{18}O^{18}O^-$ is consistent with the initial homolytic cleavage of the peroxyl bond in the adduct, formation of phenyl-type radical and $^{\bullet}NO_2$, and recombination of both radicals (Fig. 10).

2-Hydroxyethidium as a specific marker for $O_2^{\bullet-}$

The HPLC or LC-MS-based analysis of 2-OH-E^+ is regarded as a "gold standard" of the detection of $O_2^{\bullet-}$ in biological systems (77). However, the utility of 2-OH-E^+ as the marker of cellular $O_2^{\bullet-}$ recently has been questioned, based on the lack of increase of its amount in HepG2 cells treated with H_2O_2 or rotenone (78). However, the ability of those treatments to induce $O_2^{\bullet-}$ generation in the used cell model has not been shown. Numerous reports demonstrate the utility of HE, MitoSOX Red, and hydropropidine, when coupled with HPLC-based analyses, to detect $O_2^{\bullet-}$ in different cellular models, as reviewed elsewhere (20, 21, 63). In those reports, 2-OH-E^+, 2-OH-Mito-E^+, and 2-OH-Pr^{2+} were used as specific marker products for $O_2^{\bullet-}$. Hydroxylation of ethidium-based probes remains a method of choice for the detection of $O_2^{\bullet-}$ in cell-free and cellular systems (17, 22, 64–66, 79).

The presented results demonstrate that the specificity of 2-OH-E^+ for $O_2^{\bullet-}$ derives from incorporation of an oxygen atom from this species. Together with the pulse radiolysis data on the oxidation of HE by pulse-generated $O_2^{\bullet-}$ (68), the 2:1 stoichiometry of the reaction (67), and the lack of incorporation of oxygen from water, observed in this study and during oxidation of HE by Fremy's salt (80), the obtained data are consistent with the mechanism shown in Fig. 12. Initial oxidation of HE by the protonated form of $O_2^{\bullet-}$ (hydroperoxyl radical, $HO_2^{\bullet}$) produces a radical cation of HE, which rapidly reacts with $O_2^{\bullet-}$ to form a hydroperoxide, containing oxygen atoms from $O_2^{\bullet-}$ (Fig. 12). This product must undergo rapid transformation in aqueous solutions to 2-OH-E^+ as no intermediates have been detected by HPLC analyses.

Concluding remarks

In summary, we demonstrated that the oxygen atoms in the oxidation and nitration products of the boronate probe, *o*MitoPhB(OH)$_2$, originate from the corresponding oxidants, H_2O_2, HCO_4^-, HOCl, or $ONOO^-$. Also, in the case the conversion of the HE probe into 2-OH-E$^+$, oxygen comes from $O_2^{\cdot-}$. The presented data indicate that it is possible to track isotopically labeled oxidants by monitoring the incorporation of the isotopes into the oxidation/nitration products using the boronate and hydroethidine probes. Because no incorporation of the atoms from ROS/reactive nitrogen species occurs in most other commonly used probes, including DCFH, DHR123, Amplex Red, and NBT, they cannot be used for such purposes. The results obtained also corroborate the mechanisms of the conversion of HE into 2-OH-E$^+$ by $O_2^{\cdot-}$ and of oxidation and nitration of boronate-based probes, proposed previously based on product analyses, EPR experiments, and density functional theory calculation. We expect that oxygen-18 labeling studies using $^{18}O_2$, $H_2{}^{18}O$, and $H_2{}^{18}O_2$, may also be used in cell-free or cellular systems to reveal whether metal-induced hydrolysis and/or high-valent iron-oxo species may contribute to the hydroxylation of the probes (81). The reaction of the probes with ^{18}O-labeled oxidants also can be used to prepare isotopically labeled standards of the oxidation products. Furthermore, $H_2{}^{18}O_2$- or $H^{18}O_2C^{16}O_2^-$-mediated oxidation of boronates represents a convenient route for the synthesis of ^{18}O-labeled alcohols and phenols.

Experimental procedures

Materials

Ortho-MitoPhB(OH)$_2$ and its oxidation and nitration products were synthesized, as described previously (49–51). The stock solution of *o*MitoPhB(OH)$_2$ (0.1 M) was prepared in DMSO and stored at −20 °C. The HE probe was obtained from Invitrogen (Carlsbad, CA). The stock solution of HE (20 mM) was prepared in deoxygenated DMSO under argon atmosphere and stored at −80 °C. The standards of the oxidation products were synthesized, as described previously (22, 82). For experiments involving HOCl, both probes were dissolved in ethanol (EtOH) to avoid the scavenging effect of DMSO on HOCl (47). Water-^{18}O (97% oxygen-18), $H_2{}^{18}O_2$ (90% oxygen-18), $^{18}O_2$ (97% oxygen-18), HX, XO, superoxide dismutase (SOD), and catalase were obtained from Sigma-Aldrich. MPO was from Calbiochem.

Determination of the flux of $O_2^{\cdot-}$

$O_2^{\cdot-}$ was generated from the XO-catalyzed oxidation of HX in a phosphate buffer solution (25 mM, pH = 7.4) containing 0.1 mM diethylenetriamine pentaacetic acid (dtpa). The solution was continuously purged with O_2. The flux of $O_2^{\cdot-}$ was determined, as described previously (7, 83, 84), by performing the incubation in the presence of ferricytochrome *c* (50 μM) and monitoring the rate of its reduction following an increase in absorbance at 550 nm ($\Delta\epsilon = 2.1 \times 10^4\ M^{-1}\ cm^{-1}$) (85). Superoxide dismutase completely blocked the reduction of ferricytochrome *c* under the conditions used.

Determination of the flux of $^{\cdot}$NO

$^{\cdot}$NO was generated from the thermal decomposition of spermine NONOate in a phosphate buffer (25 mM, pH = 7.4) containing 0.1 mM dtpa. The flux of $^{\cdot}$NO was determined, as described previously (7, 84), by monitoring the rate of decay of spermine NONOate following a decrease in absorbance at 252 nm ($\epsilon = 8 \times 10^3\ M^{-1}cm^{-1}$). The release of two molecules of $^{\cdot}$NO per one molecule of spermine NONOate consumed was assumed in the calculations (86).

Oxidation of oMitoPhB(OH)$_2$ by H_2O_2

To analyze the product of oxidation of *o*MitoPhB(OH)$_2$ by H_2O_2, *o*MitoPhB(OH)$_2$ (20 μM) was incubated at room temperature with H_2O_2 (10 mM) for 20 min in a phosphate buffer (25 mM, pH = 7.4) containing 0.1 mM dtpa. When performing the reaction in water-^{18}O, the final concentration of $H_2{}^{18}O$ was 90% (by volume).

Oxidation of oMitoPhB(OH)$_2$ by HCO_4^-

Oxidation *o*MitoPhB(OH)$_2$ by HCO_4^- was studied by incubation of the probe with H_2O_2 in phosphate-buffered (0.1 M) aqueous solution containing dtpa (0.1 mM) in the presence of $NaHCO_3$ (25 and 50 mM). To maximize the involvement of HCO_4^- in probe oxidation, the probe concentration was lowered to 1 μM, the H_2O_2 concentration was lowered to 50 μM, and the pH was adjusted to 7.0.

Oxidation of oMitoPhB(OH)$_2$ by HOCl

To study oxidation of *o*MitoPhB(OH)$_2$ by HOCl, the probe (50 μM, from a stock solution in EtOH) was incubated with H_2O_2 (0.1 mM), KCl (0.1 M), and MPO (20 nM) for 15 min at 25 °C in a phosphate-buffered (0.1 M) aqueous solution. Where indicated, DMSO was added (final concentration of 0.2% v/v) to scavenge HOCl.

Oxidation of oMitoPhB(OH)$_2$ by $ONOO^-$

To react *o*MitoPhB(OH)$_2$ with $ONOO^-$, *o*MitoPhB(OH)$_2$ (20 μM) was incubated with spermine NONOate (200 μM, generating 0.2 μM/min $^{\cdot}$NO), HX (200 μM), and XO (0.1 milliunit/milliliter, 0.2 μM $O_2^{\cdot-}$/min) in an O_2-saturated phosphate buffer (25 mM, pH = 7.4) containing 0.1 mM dtpa and 5 kilounits/milliliter catalase. The deoxygenated stock solutions of all components were mixed under argon atmosphere in a hypoxic chamber (final reaction volume: 200 μl). The incubation was started immediately after mixing by passing oxygen gas ($^{16}O_2$ or $^{18}O_2$) through the solution for 10 min, followed by 20 min further incubation at room temperature. Incubation in water-^{18}O was performed in the presence of 90% (by volume) of $H_2{}^{18}O$.

Chlorination of HE by HOCl

The reaction of HE with HOCl and the formation of 2-Cl-E$^+$ was investigated in the presence of H_2O_2, MPO, and KCl under conditions identical to those described above for the *o*MitoPhB(OH)$_2$ probe but using HE (50 μM, from a stock solution in EtOH).

Oxidation of HE by $O_2^{\cdot-}$

Conversion of HE into 2-OH-E$^+$ was studied by incubation of HE (20 μM) with HX (200 μM) and XO (0.1 milliunit/millili-

ter, 0.2 μM $O_2^{\cdot-}$/min) in an oxygen-saturated phosphate buffer (25 mM, pH = 7.4) containing 0.1 mM dtpa and 5 kilounits/milliliter catalase. To better control the type of O_2 isotopolog present in the solutions, samples were first deoxygenated to remove $^{16}O_2$ and then reoxygenated using $^{16}O_2$ or $^{18}O_2$. The deoxygenated stock solutions of all components were mixed under argon atmosphere in a hypoxic chamber (final reaction volume 200 μl). The incubation was started immediately after mixing by passing O_2 gas ($^{16}O_2$ or $^{18}O_2$) through the solution for 10 min, followed by 20 min further incubation at room temperature. To stop the incubation, SOD was added (final concentration: 0.1 mg/ml) and the sample was taken for LC-MS/MS analysis. The addition of SOD at the beginning of incubation resulted in complete inhibition of 2-OH-E^+ formation. When using water-^{18}O as a solvent, the final concentration of $H_2{}^{18}O$ was 90% (by volume).

LC-MS/MS analysis of oMitoPhB(OH)$_2$ oxidation products

The oxidation products of *o*MitoPhB(OH)$_2$ were analyzed using a Shimadzu Nexera2 ultra-HPLC system equipped with UV-visible absorption and LC-MS8030 MS detectors (Columbia, MD). The presence of a positive charge (because of the presence of the TPP^+ moiety) allows a sensitive detection by MS, as reported previously for the MitoB probe (41–43). The incubation mixture was injected into a Raptor Biphenyl column (Restek, Bellefonte, PA; 100 mm × 2.1 mm, 2.7 μm) equilibrated with a mobile phase containing 80% water, 20% MeCN, and 0.1% formic acid. The products were eluted by increasing the content of MeCN (containing 0.1% formic acid) from 20% to 60% over 5.5 min. The mobile phase flow rate was 0.5 ml/min. Detection events included continuous scanning of the spectra of the eluate, as well as detection of the specific oxidation products in an MRM mode. MRM transitions were as follows: 397 > 135 for *o*MitoPhB(OH)$_2$, 369 > 107 for *o*MitoPh^{16}OH, 371 > 263 for *o*MitoPh^{18}OH, 398 > 262 for *o*MitoPhN$^{16}O_2$, 400 > 262 for *o*MitoPhN$^{16}O^{18}O$, and 351 > 183 for *cyclo*-*o*MitoPh. The MRM transitions of other oxidation products have been reported elsewhere (50, 51, 79).

LC-MS/MS analysis of HE oxidation products

Detection of HE oxidation products, including 2-Cl-E^+ and 2-OH-E^+, was performed using a Shimadzu Nexera2 ultra-HPLC system equipped with UV-visible absorption and LC-MS8030 MS detectors. The reaction mixture was injected into a Raptor Biphenyl column (Restek, Bellefonte, PA; 100 mm × 2.1 mm, 2.7 μm) equilibrated with the mobile phase containing 90% water, 10% acetonitrile (MeCN), and 0.1% formic acid. The products were eluted by increasing the content of the organic mobile phase (MeCN, 0.1% formic acid) from 10% to 65% over 4.5 min at the flow rate of 0.4 ml/min. Detection events included continuous scanning of the spectra of the eluate, as well as detection of the specific oxidation products in an MRM mode. MRM transitions for 2-Cl-E^+, 2-^{16}OH-E^+, and 2-^{18}OH-E^+ were 348 > 320, 330 > 300, and 332 > 302, respectively. The MRM transitions of other oxidation products were as reported previously (19, 29, 75, 79).

Data availability

All data presented and discussed are contained within the manuscript or in the supporting information.

Author contributions—N. R. and J. Z. data curation; N. R. and J. Z. formal analysis; N. R., R. R., B. K., and J. Z. funding acquisition; N. R. validation; N. R. and J. Z. investigation; N. R. and J. Z. methodology; N. R., R. R., B. K., and J. Z. writing-review and editing; R. R., B. K., and J. Z. conceptualization; R. R., B. K., and J. Z. supervision; R. R. and B. K. project administration; B. K. and J. Z. resources; J. Z. writing-original draft.

References

1. Winterbourn, C. C. (2008) Reconciling the chemistry and biology of reactive oxygen species. *Nat. Chem. Biol.* **4,** 278–286 CrossRef Medline
2. Forman, H. J., Ursini, F., and Maiorino, M. (2014) An overview of mechanisms of redox signaling. *J. Mol. Cell Cardiol.* **73,** 2–9 CrossRef Medline
3. Reczek, C. R., and Chandel, N. S. (2015) ROS-dependent signal transduction. *Curr. Opin. Cell Biol.* **33,** 8–13 CrossRef Medline
4. Winterbourn, C. C. (2018) Biological production, detection, and fate of hydrogen peroxide. *Antioxid. Redox Signal.* **29,** 541–551 CrossRef Medline
5. Vissers, M. C., Hampton, M., and Kettle, A. J. (2017) *Hydrogen Peroxide Metabolism in Health and Disease*. CRC Press, Boca Raton, FL
6. Winterbourn, C. C. (2020) Biological chemistry of superoxide radicals. *ChemTexts* **6,** 7 CrossRef
7. Zielonka, J., Sikora, A., Joseph, J., and Kalyanaraman, B. (2010) Peroxynitrite is the major species formed from different flux ratios of co-generated nitric oxide and superoxide: Direct reaction with boronate-based fluorescent probe. *J. Biol. Chem.* **285,** 14210–14216 CrossRef Medline
8. Ferrer-Sueta, G., Campolo, N., Trujillo, M., Bartesaghi, S., Carballal, S., Romero, N., Alvarez, B., and Radi, R. (2018) Biochemistry of peroxynitrite and protein tyrosine nitration. *Chem. Rev.* **118,** 1338–1408 CrossRef Medline
9. Bakhmutova-Albert, E. V., Yao, H., Denevan, D. E., and Richardson, D. E. (2010) Kinetics and mechanism of peroxymonocarbonate formation. *Inorg. Chem.* **49,** 11287–11296 CrossRef Medline
10. Truzzi, D. R., and Augusto, O. (2017) Influence of CO2 on hydroperoxide metabolism. in *Hydrogen Peroxide Metabolism in Health and Disease* (Vissers, M. C., Hampton, M., and Kettle, A. J., eds), pp. 81–99, CRC Press, Boca Raton, FL
11. Pattison, D. I., Davies, M. J., and Hawkins, C. L. (2012) Reactions and reactivity of myeloperoxidase-derived oxidants: Differential biological effects of hypochlorous and hypothiocyanous acids. *Free Radic. Res.* **46,** 975–995 CrossRef Medline
12. Dagnell, M., Cheng, Q., Rizvi, S. H. M., Pace, P. E., Boivin, B., Winterbourn, C. C., and Arnér, E. S. J. (2019) Bicarbonate is essential for protein-tyrosine phosphatase 1B (PTP1B) oxidation and cellular signaling through EGF-triggered phosphorylation cascades. *J. Biol. Chem.* **294,** 12330–12338 CrossRef Medline
13. Hawkins, C. L., and Davies, M. J. (2019) Detection, identification, and quantification of oxidative protein modifications. *J. Biol. Chem.* **294,** 19683–19708 CrossRef Medline
14. Hardy, M., Zielonka, J., Karoui, H., Sikora, A., Michalski, R., Podsiadly, R., Lopez, M., Vasquez-Vivar, J., Kalyanaraman, B., and Ouari, O. (2018) Detection and characterization of reactive oxygen and nitrogen species in biological systems by monitoring species-specific products. *Antioxid. Redox Signal.* **28,** 1416–1432 CrossRef Medline
15. Kalyanaraman, B., Hardy, M., Podsiadly, R., Cheng, G., and Zielonka, J. (2017) Recent developments in detection of superoxide radical anion and hydrogen peroxide: Opportunities, challenges, and implications in redox signaling. *Arch. Biochem. Biophys.* **617,** 38–47 CrossRef Medline

16. Zielonka, J., and Kalyanaraman, B. (2018) Small-molecule luminescent probes for the detection of cellular oxidizing and nitrating species. *Free Radic. Biol. Med.* **128,** 3–22 CrossRef Medline
17. Dikalov, S. I., and Harrison, D. G. (2014) Methods for detection of mitochondrial and cellular reactive oxygen species. *Antioxid. Redox Signal.* **20,** 372–382 CrossRef Medline
18. Debowska, K., Debski, D., Hardy, M., Jakubowska, M., Kalyanaraman, B., Marcinek, A., Michalski, R., Michalowski, B., Ouari, O., Sikora, A., Smulik, R., and Zielonka, J. (2015) Toward selective detection of reactive oxygen and nitrogen species with the use of fluorogenic probes—limitations, progress, and perspectives. *Pharmacol. Rep.* **67,** 756–764 CrossRef Medline
19. Koto, T., Michalski, R., Zielonka, J., Joseph, J., and Kalyanaraman, B. (2014) Detection and identification of oxidants formed during *NO/O2*(−) reaction: A multi-well plate CW-EPR spectroscopy combined with HPLC analyses. *Free Radic. Res.* **48,** 478–486 CrossRef Medline
20. Kalyanaraman, B., Dranka, B. P., Hardy, M., Michalski, R., and Zielonka, J. (2014) HPLC-based monitoring of products formed from hydroethidine-based fluorogenic probes—the ultimate approach for intra- and extracellular superoxide detection. *Biochim. Biophys. Acta* **1840,** 739–744 CrossRef Medline
21. Zielonka, J., and Kalyanaraman, B. (2010) Hydroethidine- and MitoSOX-derived red fluorescence is not a reliable indicator of intracellular superoxide formation: Another inconvenient truth. *Free Radic. Biol. Med.* **48,** 983–1001 CrossRef Medline
22. Zielonka, J., Vasquez-Vivar, J., and Kalyanaraman, B. (2008) Detection of 2-hydroxyethidium in cellular systems: A unique marker product of superoxide and hydroethidine. *Nat. Protoc.* **3,** 8–21 CrossRef Medline
23. Zhao, H., Joseph, J., Fales, H. M., Sokoloski, E. A., Levine, R. L., Vasquez-Vivar, J., and Kalyanaraman, B. (2005) Detection and characterization of the product of hydroethidine and intracellular superoxide by HPLC and limitations of fluorescence. *Proc. Natl. Acad. Sci. U.S.A.* **102,** 5727–5732 CrossRef Medline
24. Zhao, H., Kalivendi, S., Zhang, H., Joseph, J., Nithipatikom, K., Vásquez-Vivar, J., and Kalyanaraman, B. (2003) Superoxide reacts with hydroethidine but forms a fluorescent product that is distinctly different from ethidium: Potential implications in intracellular fluorescence detection of superoxide. *Free Radic. Biol. Med.* **34,** 1359–1368 CrossRef Medline
25. Proniewski, B., Kij, A., Sitek, B., Kelley, E. E., and Chlopicki, S. (2019) Multiorgan development of oxidative and nitrosative stress in LPS-induced endotoxemia in C57Bl/6 mice: DHE-based in vivo approach. *Oxid. Med. Cell. Longev.* **2019,** 7838406 CrossRef Medline
26. Seredenina, T., Nayernia, Z., Sorce, S., Maghzal, G. J., Filippova, A., Ling, S. C., Basset, O., Plastre, O., Daali, Y., Rushing, E. J., Giordana, M. T., Cleveland, D. W., Aguzzi, A., Stocker, R., Krause, K. H., and Jaquet, V. (2016) Evaluation of NADPH oxidases as drug targets in a mouse model of familial amyotrophic lateral sclerosis. *Free Radic. Biol. Med.* **97,** 95–108 CrossRef Medline
27. Fernandes, D. C., Wosniak, J., Jr., Pescatore, L. A., Bertoline, M. A., Liberman, M., Laurindo, F. R., and Santos, C. X. (2007) Analysis of DHE-derived oxidation products by HPLC in the assessment of superoxide production and NADPH oxidase activity in vascular systems. *Am. J. Physiol. Cell Physiol.* **292,** C413–C422 CrossRef Medline
28. Zielonka, J., Srinivasan, S., Hardy, M., Ouari, O., Lopez, M., Vasquez-Vivar, J., Avadhani, N. G., and Kalyanaraman, B. (2008) Cytochrome c-mediated oxidation of hydroethidine and mito-hydroethidine in mitochondria: Identification of homo- and heterodimers. *Free Radic. Biol. Med.* **44,** 835–846 CrossRef Medline
29. Maghzal, G. J., Cergol, K. M., Shengule, S. R., Suarna, C., Newington, D., Kettle, A. J., Payne, R. J., and Stocker, R. (2014) Assessment of myeloperoxidase activity by the conversion of hydroethidine to 2-chloroethidium. *J. Biol. Chem.* **289,** 5580–5595 CrossRef Medline
30. Lippert, A. R., Van de Bittner, G. C., and Chang, C. J. (2011) Boronate oxidation as a bioorthogonal reaction approach for studying the chemistry of hydrogen peroxide in living systems. *Acc. Chem. Res.* **44,** 793–804 CrossRef Medline
31. Lin, V. S., Dickinson, B. C., and Chang, C. J. (2013) Boronate-based fluorescent probes: Imaging hydrogen peroxide in living systems. *Methods Enzymol.* **526,** 19–43 CrossRef Medline
32. Zielonka, J., Cheng, G., Zielonka, M., Ganesh, T., Sun, A., Joseph, J., Michalski, R., O'Brien, W. J., Lambeth, J. D., and Kalyanaraman, B. (2014) High-throughput assays for superoxide and hydrogen peroxide: Design of a screening workflow to identify inhibitors of NADPH oxidases. *J. Biol. Chem.* **289,** 16176–16189 CrossRef Medline
33. Carroll, V., Michel, B. W., Blecha, J., VanBrocklin, H., Keshari, K., Wilson, D., and Chang, C. J. (2014) A boronate-caged [^{18}F]FLT probe for hydrogen peroxide detection using positron emission tomography. *J. Am. Chem. Soc.* **136,** 14742–14745 CrossRef Medline
34. Van de Bittner, G. C., Dubikovskaya, E. A., Bertozzi, C. R., and Chang, C. J. (2010) In vivo imaging of hydrogen peroxide production in a murine tumor model with a chemoselective bioluminescent reporter. *Proc. Natl. Acad. Sci. U.S.A.* **107,** 21316–21321 CrossRef Medline
35. Lippert, A. R., Gschneidtner, T., and Chang, C. J. (2010) Lanthanide-based luminescent probes for selective time-gated detection of hydrogen peroxide in water and in living cells. *Chem. Commun.* **46,** 7510–7512 CrossRef Medline
36. Seven, O., Sozmen, F., and Turan, I. S. (2017) Self immolative dioxetane based chemiluminescent probe for H_2O_2 detection. *Sensors and Actuators B: Chemical* **239,** 1318–1324 CrossRef
37. Dickinson, B. C., Huynh, C., and Chang, C. J. (2010) A palette of fluorescent probes with varying emission colors for imaging hydrogen peroxide signaling in living cells. *J. Am. Chem. Soc.* **132,** 5906–5915 CrossRef Medline
38. Srikun, D., Albers, A. E., Nam, C. I., Iavarone, A. T., and Chang, C. J. (2010) Organelle-targetable fluorescent probes for imaging hydrogen peroxide in living cells via SNAP-Tag protein labeling. *J. Am. Chem. Soc.* **132,** 4455–4465 CrossRef Medline
39. Xiao, H., Li, P., Hu, X., Shi, X., Zhang, W., and Tang, B. (2016) Simultaneous fluorescence imaging of hydrogen peroxide in mitochondria and endoplasmic reticulum during apoptosis. *Chem. Sci.* **7,** 6153–6159 CrossRef Medline
40. Dickinson, B. C., Lin, V. S., and Chang, C. J. (2013) Preparation and use of MitoPY1 for imaging hydrogen peroxide in mitochondria of live cells. *Nat. Protoc.* **8,** 1249–1259 CrossRef Medline
41. Cairns, A. G., McQuaker, S. J., Murphy, M. P., and Hartley, R. C. (2015) Targeting mitochondria with small molecules: The preparation of MitoB and MitoP as exomarkers of mitochondrial hydrogen peroxide. *Methods Mol. Biol.* **1265,** 25–50 CrossRef Medline
42. Cochemé, H. M., Quin, C., McQuaker, S. J., Cabreiro, F., Logan, A., Prime, T. A., Abakumova, I., Patel, J. V., Fearnley, I. M., James, A. M., Porteous, C. M., Smith, R. A., Saeed, S., Carré, J. E., Singer, M., Gems, D., Hartley, R. C., Partridge, L., and Murphy, M. P. (2011) Measurement of H2O2 within living Drosophila during aging using a ratiometric mass spectrometry probe targeted to the mitochondrial matrix. *Cell Metab.* **13,** 340–350 CrossRef Medline
43. Cochemé, H. M., Logan, A., Prime, T. A., Abakumova, I., Quin, C., McQuaker, S. J., Patel, J. V., Fearnley, I. M., James, A. M., Porteous, C. M., Smith, R. A., Hartley, R. C., Partridge, L., and Murphy, M. P. (2012) Using the mitochondria-targeted ratiometric mass spectrometry probe MitoB to measure H2O2 in living Drosophila. *Nat. Protoc.* **7,** 946–958 CrossRef Medline
44. Sikora, A., Zielonka, J., Lopez, M., Joseph, J., and Kalyanaraman, B. (2009) Direct oxidation of boronates by peroxynitrite: Mechanism and implications in fluorescence imaging of peroxynitrite. *Free Radic. Biol. Med.* **47,** 1401–1407 CrossRef Medline
45. Sikora, A., Zielonka, J., Lopez, M., Dybala-Defratyka, A., Joseph, J., Marcinek, A., and Kalyanaraman, B. (2011) Reaction between peroxynitrite and boronates: EPR spin-trapping, HPLC analyses, and quantum mechanical study of the free radical pathway. *Chem. Res. Toxicol.* **24,** 687–697 CrossRef Medline
46. Zielonka, J., Zielonka, M., Sikora, A., Adamus, J., Joseph, J., Hardy, M., Ouari, O., Dranka, B. P., and Kalyanaraman, B. (2012) Global profiling of reactive oxygen and nitrogen species in biological systems: High-throughput real-time analyses. *J. Biol. Chem.* **287,** 2984–2995 CrossRef Medline
47. Zielonka, J., Podsiadły, R., Zielonka, M., Hardy, M., and Kalyanaraman, B. (2016) On the use of peroxy-caged luciferin (PCL-1) probe for biolumi-

nescent detection of inflammatory oxidants *in vitro* and *in vivo*. Identification of reaction intermediates and oxidant-specific minor products. *Free Radic. Biol. Med.* **99,** 32–42 CrossRef Medline
48. Prolo, C., Rios, N., Piacenza, L., Álvarez, M. N., and Radi, R. (2018) Fluorescence and chemiluminescence approaches for peroxynitrite detection. *Free Radic. Biol. Med.* **128,** 59–68 CrossRef Medline
49. Zielonka, J., Joseph, J., Sikora, A., and Kalyanaraman, B. (2013) Real-time monitoring of reactive oxygen and nitrogen species in a multiwell plate using the diagnostic marker products of specific probes. *Methods Enzymol.* **526,** 145–157 CrossRef Medline
50. Zielonka, J., Sikora, A., Adamus, J., and Kalyanaraman, B. (2015) Detection and differentiation between peroxynitrite and hydroperoxides using mitochondria-targeted arylboronic acid. *Methods Mol. Biol.* **1264,** 171–181 CrossRef Medline
51. Zielonka, J., Zielonka, M., VerPlank, L., Cheng, G., Hardy, M., Ouari, O., Ayhan, M. M., Podsiadły, R., Sikora, A., Lambeth, J. D., and Kalyanaraman, B. (2016) Mitigation of NADPH oxidase 2 activity as a strategy to inhibit peroxynitrite formation. *J. Biol. Chem.* **291,** 7029–7044 CrossRef Medline
52. Richardson, D. E., Yao, H., Frank, K. M., and Bennett, D. A. (2000) Equilibria, kinetics, and mechanism in the bicarbonate activation of hydrogen peroxide: Oxidation of sulfides by peroxymonocarbonate. *J. Am. Chem. Soc.* **122,** 1729–1739 CrossRef
53. Bennett, D. A., Yao, H., and Richardson, D. E. (2001) Mechanism of sulfide oxidations by peroxymonocarbonate. *Inorg. Chem.* **40,** 2996–3001 CrossRef Medline
54. Peskin, A. V., Pace, P. E., and Winterbourn, C. C. (2019) Enhanced hyperoxidation of peroxiredoxin 2 and peroxiredoxin 3 in the presence of bicarbonate/CO_2. *Free Radic. Biol. Med.* **145,** 1–7 CrossRef Medline
55. Zhou, H., Singh, H., Parsons, Z. D., Lewis, S. M., Bhattacharya, S., Seiner, D. R., LaButti, J. N., Reilly, T. J., Tanner, J. J., and Gates, K. S. (2011) The biological buffer bicarbonate/CO_2 potentiates H_2O_2-mediated inactivation of protein tyrosine phosphatases. *J. Am. Chem. Soc.* **133,** 15803–15805 CrossRef Medline
56. Truzzi, D. R., Coelho, F. R., Paviani, V., Alves, S. V., Netto, L. E. S., and Augusto, O. (2019) The bicarbonate/carbon dioxide pair increases hydrogen peroxide-mediated hyperoxidation of human peroxiredoxin 1. *J. Biol. Chem.* **294,** 14055–14067 CrossRef Medline
57. Zielonka, J., Sikora, A., Hardy, M., Joseph, J., Dranka, B. P., and Kalyanaraman, B. (2012) Boronate probes as diagnostic tools for real time monitoring of peroxynitrite and hydroperoxides. *Chem. Res. Toxicol.* **25,** 1793–1799 CrossRef Medline
58. Kabeya, L. M., Andrade, M. F., Piatesi, F., Azzolini, A. E., Polizello, A. C., and Lucisano-Valim, Y. M. (2013) 3,3′,5,5′-tetramethylbenzidine in hypochlorous acid and taurine chloramine scavenging assays: interference of dimethyl sulfoxide and other vehicles. *Anal. Biochem.* **437,** 130–132 CrossRef Medline
59. Cheng, G., Zielonka, J., Dranka, B. P., McAllister, D., Mackinnon, A. C., Jr., Joseph, J., and Kalyanaraman, B. (2012) Mitochondria-targeted drugs synergize with 2-deoxyglucose to trigger breast cancer cell death. *Cancer Res.* **72,** 2634–2644 CrossRef Medline
60. Prolo, C., Álvarez, M. N., Ríos, N., Peluffo, G., Radi, R., and Romero, N. (2015) Nitric oxide diffusion to red blood cells limits extracellular, but not intraphagosomal, peroxynitrite formation by macrophages. *Free Radic. Biol. Med.* **87,** 346–355 CrossRef Medline
61. Ríos, N., Piacenza, L., Trujillo, M., Martínez, A., Demicheli, V., Prolo, C., Álvarez, M. N., López, G. V., and Radi, R. (2016) Sensitive detection and estimation of cell-derived peroxynitrite fluxes using fluorescein-boronate. *Free Radic. Biol. Med.* **101,** 284–295 CrossRef Medline
62. Smulik, R., Dębski, D., Zielonka, J., Michałowski, B., Adamus, J., Marcinek, A., Kalyanaraman, B., and Sikora, A. (2014) Nitroxyl (HNO) reacts with molecular oxygen and forms peroxynitrite at physiological pH. Biological implications. *J. Biol. Chem.* **289,** 35570–35581 CrossRef Medline
63. Zielonka, J., Hardy, M., Michalski, R., Sikora, A., Zielonka, M., Cheng, G., Ouari, O., Podsiadły, R., and Kalyanaraman, B. (2017) Recent developments in the probes and assays for measurement of the activity of NADPH oxidases. *Cell Biochem. Biophys.* **75,** 335–349 CrossRef Medline
64. Robinson, K. M., Janes, M. S., Pehar, M., Monette, J. S., Ross, M. F., Hagen, T. M., Murphy, M. P., and Beckman, J. S. (2006) Selective fluorescent imaging of superoxide *in vivo* using ethidium-based probes. *Proc. Natl. Acad. Sci. U.S.A.* **103,** 15038–15043 CrossRef Medline
65. Michalski, R., Zielonka, J., Hardy, M., Joseph, J., and Kalyanaraman, B. (2013) Hydropropidine: A novel, cell-impermeant fluorogenic probe for detecting extracellular superoxide. *Free Radic. Biol. Med.* **54,** 135–147 CrossRef Medline
66. Shchepinova, M. M., Cairns, A. G., Prime, T. A., Logan, A., James, A. M., Hall, A. R., Vidoni, S., Arndt, S., Caldwell, S. T., Prag, H. A., Pell, V. R., Krieg, T., Mulvey, J. F., Yadav, P., Cobley, J. N., *et al*. (2017) MitoNeoD: A mitochondria-targeted superoxide probe. *Cell Chem. Biol.* **24,** 1285–1298.e1212 CrossRef Medline
67. Michalski, R., Michalowski, B., Sikora, A., Zielonka, J., and Kalyanaraman, B. (2014) On the use of fluorescence lifetime imaging and dihydroethidium to detect superoxide in intact animals and *ex vivo* tissues: A reassessment. *Free Radic. Biol. Med.* **67,** 278–284 CrossRef Medline
68. Zielonka, J., Sarna, T., Roberts, J. E., Wishart, J. F., and Kalyanaraman, B. (2006) Pulse radiolysis and steady-state analyses of the reaction between hydroethidine and superoxide and other oxidants. *Arch. Biochem. Biophys.* **456,** 39–47 CrossRef Medline
69. Rinkel, J., and Dickschat, J. S. (2015) Recent highlights in biosynthesis research using stable isotopes. *Beilstein J. Org. Chem.* **11,** 2493–2508 CrossRef Medline
70. Lehmann, W. D. (2017) A timeline of stable isotopes and mass spectrometry in the life sciences. *Mass Spectrom. Rev.* **36,** 58–85 CrossRef Medline
71. Jang, C., Chen, L., and Rabinowitz, J. D. (2018) Metabolomics and isotope tracing. *Cell* **173,** 822–837 CrossRef Medline
72. Mottley, C., Connor, H. D., and Mason, R. P. (1986) [^{17}O]oxygen hyperfine structure for the hydroxyl and superoxide radical adducts of the spin traps DMPO, PBN and 4-POBN. *Biochem. Biophys. Res. Commun.* **141,** 622–628 CrossRef Medline
73. Michalski, R., Zielonka, J., Gapys, E., Marcinek, A., Joseph, J., and Kalyanaraman, B. (2014) Real-time measurements of amino acid and protein hydroperoxides using coumarin boronic acid. *J. Biol. Chem.* **289,** 22536–22553 CrossRef Medline
74. Wardman, P. (2008) Methods to measure the reactivity of peroxynitrite-derived oxidants toward reduced fluoresceins and rhodamines. *Methods Enzymol.* **441,** 261–282 CrossRef Medline
75. Talib, J., Maghzal, G. J., Cheng, D., and Stocker, R. (2016) Detailed protocol to assess *in vivo* and *ex vivo* myeloperoxidase activity in mouse models of vascular inflammation and disease using hydroethidine. *Free Radic. Biol. Med.* **97,** 124–135 CrossRef Medline
76. Sedgwick, A. C., Dou, W. T., Jiao, J. B., Wu, L., Williams, G. T., Jenkins, A. T. A., Bull, S. D., Sessler, J. L., He, X. P., and James, T. D. (2018) An ESIPT probe for the ratiometric imaging of peroxynitrite facilitated by binding to Aβ-aggregates. *J. Am. Chem. Soc.* **140,** 14267–14271 CrossRef Medline
77. Dikalov, S., Griendling, K. K., and Harrison, D. G. (2007) Measurement of reactive oxygen species in cardiovascular studies. *Hypertension* **49,** 717–727 CrossRef Medline
78. Xiao, Y., and Meierhofer, D. (2019) Are hydroethidine-based probes reliable for reactive oxygen species detection? *Antioxid. Redox Signal.* **31,** 359–367 CrossRef Medline
79. Cheng, G., Zielonka, M., Dranka, B., Kumar, S. N., Myers, C. R., Bennett, B., Garces, A. M., Dias Duarte Machado, L. G., Thiebaut, D., Ouari, O., Hardy, M., Zielonka, J., and Kalyanaraman, B. (2018) Detection of mitochondria-generated reactive oxygen species in cells using multiple probes and methods: Potentials, pitfalls, and the future. *J. Biol. Chem.* **293,** 10363–10380 CrossRef Medline
80. Zielonka, J., Zhao, H., Xu, Y., and Kalyanaraman, B. (2005) Mechanistic similarities between oxidation of hydroethidine by Fremy's salt and superoxide: Stopped-flow optical and EPR studies. *Free Radic. Biol. Med.* **39,** 853–863 CrossRef Medline
81. Shan, X., and Que, L. (2006) High-valent nonheme iron-oxo species in biomimetic oxidations. *J. Inorg. Biochem.* **100,** 421–433 CrossRef Medline
82. Zielonka, J., Hardy, M., and Kalyanaraman, B. (2009) HPLC study of oxidation products of hydroethidine in chemical and biological systems: ramifications in superoxide measurements. *Free Radic. Biol. Med.* **46,** 329–338 CrossRef Medline

83. Rubbo, H., Radi, R., Trujillo, M., Telleri, R., Kalyanaraman, B., Barnes, S., Kirk, M., and Freeman, B. A. (1994) Nitric oxide regulation of superoxide and peroxynitrite-dependent lipid peroxidation. Formation of novel nitrogen-containing oxidized lipid derivatives. *J. Biol. Chem.* **269,** 26066–26075 Medline
84. Alvarez, M. N., Trujillo, M., and Radi, R. (2002) Peroxynitrite formation from biochemical and cellular fluxes of nitric oxide and superoxide. *Methods Enzymol.* **359,** 353–366 CrossRef Medline
85. Massey, V. (1959) The microestimation of succinate and the extinction coefficient of cytochrome c. *Biochim. Biophys. Acta* **34,** 255–256 CrossRef Medline
86. Thomas, D. D., Miranda, K. M., Espey, M. G., Citrin, D., Jourd'heuil, D., Paolocci, N., Hewett, S. J., Colton, C. A., Grisham, M. B., Feelisch, M., and Wink, D. A. (2002) Guide for the use of nitric oxide (NO) donors as probes of the chemistry of NO and related redox species in biological systems. *Methods Enzymol.* **359,** 84–105 CrossRef Medline